nature genetics

Mutations in the gene encoding pejvakin, a newly identified protein of the afferent auditory pathway, cause DFNB59 auditory neuropathy

Sedigheh Delmaghani[1], Francisco J del Castillo[1], Vincent Michel[1], Michel Leibovici[1], Asadollah Aghaie[1], Uri Ron[2], Lut Van Laer[3], Nir Ben-Tal[2], Guy Van Camp[3], Dominique Weil[1], Francina Langa[4], Mark Lathrop[5], Paul Avan[6] & Christine Petit[1]

Auditory neuropathy is a particular type of hearing impairment in which neural transmission of the auditory signal is impaired, while cochlear outer hair cells remain functional. Here we report on *DFNB59*, a newly identified gene on chromosome 2q31.1–q31.3 mutated in four families segregating autosomal recessive auditory neuropathy. *DFNB59* encodes pejvakin, a 352-residue protein. Pejvakin is a paralog of DFNA5, a protein of unknown function also involved in deafness. By immunohistofluorescence, pejvakin is detected in the cell bodies of neurons of the afferent auditory pathway. Furthermore, *Dfnb59* knock-in mice, homozygous for the R183W variant identified in one DFNB59 family, show abnormal auditory brainstem responses indicative of neuronal dysfunction along the auditory pathway. Unlike previously described sensorineural deafness genes, all of which underlie cochlear cell pathologies, *DFNB59* is the first human gene implicated in nonsyndromic deafness due to a neuronal defect.

The mammalian hearing organ, the cochlea, consists of a coiled, fluid-filled membranous duct that contains the sensory epithelium responsive to sound. This sensory epithelium, termed the organ of Corti, comprises two different kinds of sensory cells, inner hair cells (IHCs) and outer hair cells (OHCs), that are surrounded by supporting cells. The apical specialization of hair cells, the hair bundle, houses the mechanotransductive machinery that transforms sound-induced mechanical stimuli into cell depolarization. This results in neurotransmitter release and the generation in spiral ganglion neurons (auditory nerve) of action potentials that are relayed by the brainstem to the auditory cortex. Each class of sensory cell serves a different function. IHCs are the genuine sound receptors, whereas OHCs behave as active mechanical effectors that impart high sensitivity, sharp tuning and wide dynamic range to the cochlea. This functional difference is also evident in the afferent innervation of hair cells. Each single IHC is innervated by 15–20 type I spiral ganglion neurons that provide very quick, parallel channels for transmitting auditory information to the brain. In contrast, 30–60 OHCs are innervated by a single type II spiral ganglion neuron, thus integrating the sensory input from many different effector cells[1,2]. The basic auditory signal conveyed by spiral ganglion neurons is analyzed, decoded and integrated along the afferent auditory pathway, which includes four major relays (cochlear nuclei, superior olive, inferior colliculus and medial geniculate body) before reaching the auditory cortex in the temporal lobe of the brain[3]. Each level in the auditory pathway is tonotopically organized, paralleling the distribution of the range of sound frequencies perceived along the cochlear spiral, from base (high frequencies) to apex (low frequencies)[3,4].

Most forms of inherited sensorineural hearing impairment are due to cochlear cell defects. However, a substantial proportion of cases, including up to 10% of all cases of permanent hearing impairment in children[5], are caused by a lesion located beyond the cochlea. Clinical tests for sensorineural hearing impairment include recording the auditory brainstem response (ABR), which measures the acoustic stimulus–evoked electrophysiological response of the auditory nerve and brainstem[6], and otoacoustic emissions (OAEs), which are low-level sounds originating in the cochlea due to the mechanical activity of OHCs[7]. Auditory neuropathy is a type of sensorineural hearing impairment in which the ABR is absent or severely distorted while OAEs are preserved[8]. This suggests a primary lesion located in the IHC, in the auditory nerve or in the intervening synapse[9,10], but may also include damage to neuronal populations in the auditory pathway[9].

We report here the identification of the *DFNB59* gene, which underlies autosomal recessive auditory neuropathy in four consanguineous families. We also describe a *Dfnb59* knock-in mouse model of auditory neuropathy whose abnormal ABRs show impairment of

[1]Unité de Génétique des Déficits Sensoriels INSERM U587, Institut Pasteur, 25, rue du Docteur Roux, 75724 Paris Cedex 15, France. [2]Department of Biochemistry, George S. Wise Faculty of Life Sciences, Tel-Aviv University, Tel Aviv, Israel. [3]Department of Medical Genetics, University of Antwerp, Antwerp, Belgium. [4]Centre d'Ingénierie Génétique Murine, Institut Pasteur, Paris, France. [5]Centre National de Génotypage, Evry, France. [6]Laboratoire de Biophysique Sensorielle, Faculté de Médecine, Université d'Auvergne, Clermont-Ferrand, France. Correspondence should be addressed to C.P. (cpetit@pasteur.fr).

Received 20 January; accepted 25 May; published online 25 June 2006; doi:10.1038/ng1829

neural transmission. The product of *DFNB59*, pejvakin, is expressed in all the relays of the afferent auditory pathway from the cochlea to the midbrain. Altogether, our results suggest a critical role for pejvakin in the physiology of auditory neurons.

RESULTS

Clinical features

We ascertained two five-generation consanguineous families (families 705 and 312), from isolated villages located in different regions in Iran, with autosomal recessive, non-syndromic, bilateral, prelingual sensorineural hearing impairment (**Fig. 1**). In family 705, affected individuals present with profound deafness involving all frequencies that impedes speech acquisition. In family 312, pure-tone audiometry in affected subjects showed flat audiograms with hearing levels characteristic of severe hearing impairment (**Fig. 2a** and **Supplementary Note** online).

We further characterized the hearing impairment in 12 affected individuals from the two families by recording ABRs and synchronized spontaneous OAEs (SSOAEs). ABRs and ipsilateral stapedial reflexes were absent in all four subjects from family 705 and two subjects from family 312. In the six remaining subjects, all belonging to family 312, ABR thresholds were 80 dB (three subjects), 90 dB (one subject) and 100 dB (two subjects) (**Fig. 2b**), with ipsilateral stapedial reflexes present in 7 of 12 ears. Notably, these six affected individuals showed a pathological increase in the latency of wave V, the only wave that could be recognized in their ABRs (6.0–6.3 ms, compared

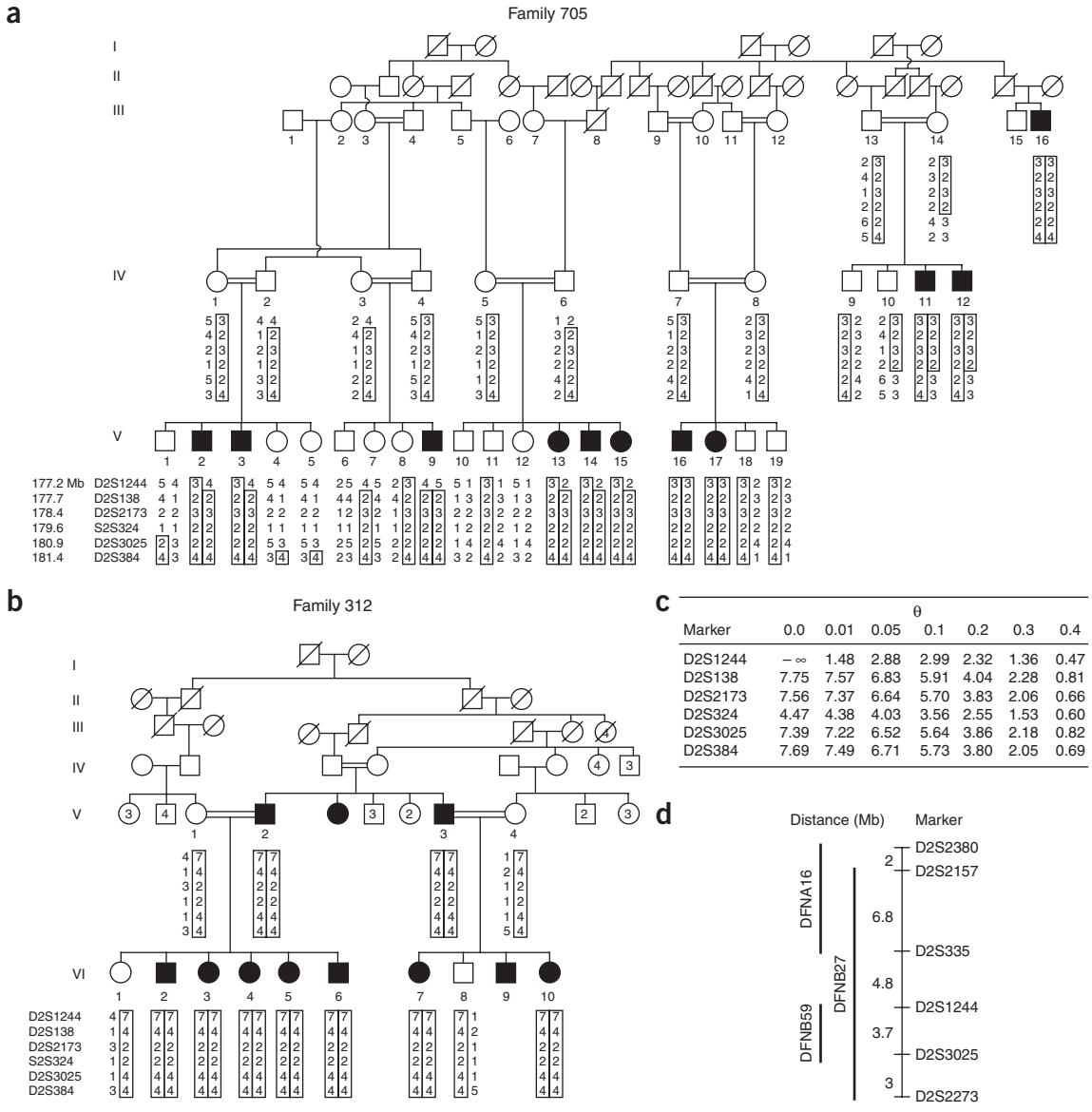

Figure 1 Mapping the *DFNB59* locus. (**a**,**b**) Pedigree and segregation analyses of families 705 (**a**) and 312 (**b**). The complete family 705 consists of 60 members, but only those relevant to the study are shown. Haplotypes are represented as columns of numbers, with the ancestral, disease-associated haplotype boxed. The column on the extreme left indicates the physical distance of each microsatellite marker from the centrosome of chromosome 2. Filled and open symbols denote hearing-impaired and unaffected individuals, respectively. (**c**) Two-point lod scores between 2q31.1–q31.3 polymorphic markers and the *DFNB59* locus in family 705. (**d**) Critical intervals for the three hearing impairment loci (*DFNA16*, *DFNB27*, and *DFNB59*) mapped to chromosomal region 2q31.

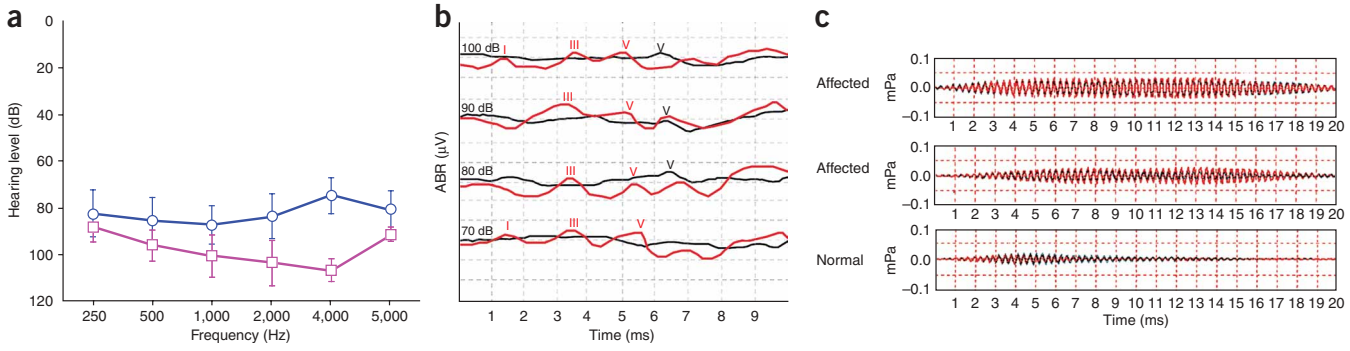

Figure 2 Audiological characterization of affected individuals with mutations in the *DFNB59* gene. (**a**) Mean audiometric hearing thresholds for all tested members of families 312 (blue circles) and 705 (purple squares). The binaural mean pure-tone averages of thresholds for air conduction at frequencies 0.5, 1 and 2 kHz ($PTA_{0.5,\ 1,\ 2\ kHz}$) are 84.7 ± 10.3 dB (family 312) and 102.2 ± 7.4 dB (family 705). (**b**) Click-evoked ABR waveforms at different sound intensities recorded in subject VI-6 of family 312 (black), compared to a control individual (red). The peaks of ABR waves I, III and V are indicated. Note the increased latency of wave V, the only wave that could be recognized in the affected individual. (**c**) SSOAE records at 3 kHz for affected individuals V-9 of family 705 (top), VI-3 of family 312 (middle) and a control individual (bottom). All of them show preserved SSOAEs. SSOAEs are spontaneous, long-lasting (up to 20 ms) ringing sounds emitted by the cochlea that are synchronized to an external stimulus and recorded by using time-averaging procedures. SSOAEs are so stable in amplitude (up to 20 dB SPL) and frequency that repeated recordings overlap almost completely (blue and red traces in each record). Preserved SSOAEs, regardless of their amplitude, indicate normal function of OHCs responding to the frequencies revealed in the SSOAEs.

with a maximum latency of 5.4 ms at 80 dB in normal-hearing control individuals, analyzed with the same equipment). In contrast, we recorded high-amplitude SSOAEs bilaterally in 11 of 12 subjects (**Fig. 2c**). These findings meet the diagnostic criteria for auditory neuropathy[8].

Mapping the *DFNB59* locus

We obtained DNA samples from 34 members of family 705 who were available for the study, including 11 affected individuals. Individuals were genotyped for a set of 400 microsatellite markers that were evenly spaced along the whole genome at intervals of 10–12 cM. We found evidence of linkage to marker D2S364 on chromosome 2q31.1-q31.3. Haplotype analysis showed that all affected individuals were homozygous for additional markers in this region, and it defined a critical interval of 3.7 Mb between markers D2S1244 and D2S3025 (**Fig. 1a**) for the newly identified deafness locus, *DFNB59*, with a maximum lod score of 7.75 at $\theta = 0.0$ for marker D2S138 (**Fig. 1c**). Of note, the interval for the *DFNB59* locus was completely contained within the critical interval reported for recessive hearing impairment locus *DFNB27* (ref. 11) (**Fig. 1d**).

Additional linkage analyses established that deafness segregated with *DFNB59* markers in family 312 (**Fig. 1b**), and in two other Iranian families (700 and 710) that originate from the same geographical area than family 705 (**Supplementary Fig. 1** online).

Identification of the *DFNB59* gene

Twelve known genes and as many ESTs mapped to the genomic region delimited by markers D2S1244 and D2S3025 (**Fig. 3a**). We conducted an exon-by-exon search for mutations in each of these genes by sequencing PCR-amplified exons from affected individual IV-11 in family 705. We did not find any disease-causing mutations in any of the known genes within the interval. In contrast, we identified a

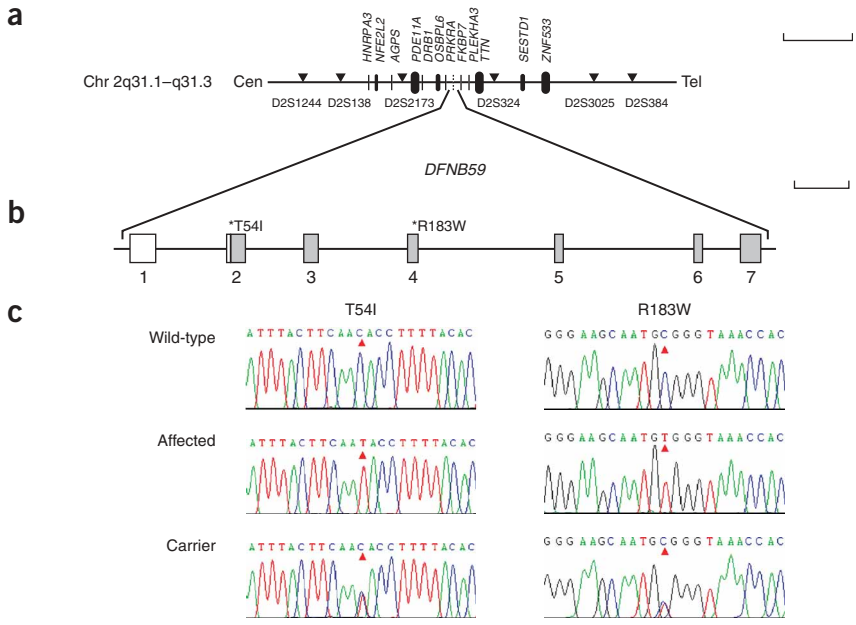

Figure 3 Genomic structure of *DFNB59*. (**a**) Physical map of the region containing *DFNB59* on chromosome 2q31.1–q31.3 (UCSC database, May 2004 release). The positions of the microsatellite markers genotyped in this work are shown by arrowheads. Known genes within this interval are depicted as boxes. Scale bar, 1 Mb. (**b**) Exon-intron structure of *DFNB59*, which consists of seven exons (boxes) spanning 9.8 kb. The *DFNB59* coding sequence is shaded. Asterisks indicate the position of the two missense mutations, resulting in amino acid changes T54I and R183W, identified in affected individuals. Scale bar: 1 kb. (**c**) Sequence electropherograms of wild-type, affected and carrier individuals for each of the two *DFNB59* mutations described in this work.

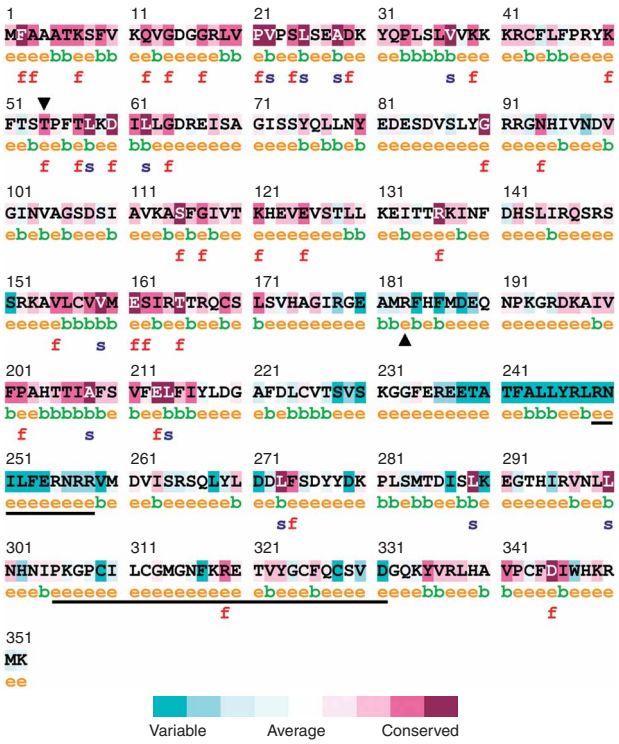

Figure 4 CONSEQ conservation analysis of human pejvakin based on the alignment of the 53 full-length members of the pejvakin-DFNA5-gasdermin-MLZE family known to date. Colors indicate the degree of conservation of each residue. The putative nuclear localization signal (residues 249–258) and zinc-binding motif (residues 305–331) are underlined. Abbreviations used: b, buried; e, exposed; f, functional; s, structural. Arrowheads indicate the two residues (Thr54 and Arg183) altered in individuals with DFNB59 auditory neuropathy.

homozygous C-to-T transition (**Fig. 3c**) in hypothetical gene BC020859 that would result in the replacement of an arginine residue with tryptophan in the predicted BC020859 polypeptide sequence. Then, we verified that this C-to-T transition segregated with the disease by sequencing BC020859 in all the remaining members of family 705.

The transcript from database entry BC020859 lacked a Kozak translation initiation sequence, suggesting that it did not represent a full-length cDNA. Thus, we identified its putative mouse ortholog by querying the EST databases for sequence similarity to BC020859. We then carried out 5′-RACE experiments on total RNA extracted from mouse inner ear in order to obtain the full-length mouse cDNA sequence. Alignment of the mouse cDNA sequence with human genomic sequences provided the potential genomic structure of the gene mutated in DFNB59 affected individuals. We used this information to design primers for the screening of a human testis cDNA library, from which we reconstructed the complete human transcript. We named the gene *DFNB59* and named the protein it encodes 'pejvakin', after the Persian word for 'echo'.

The *DFNB59* gene consists of seven exons, spanning 9.8 kb of genomic sequence (**Fig. 3b**), and codes for a 352-residue protein (deduced molecular weight, 39.9 kDa; isoelectric point, 9.31). The mutation detected in family 705 corresponds to the replacement of arginine 183 with tryptophan (547C→T; R183W) in human pejvakin.

The identification of *DFNB59* as the causative gene in DFNB59 auditory neuropathy was further substantiated by finding *DFNB59* mutations in hearing-impaired subjects from families 312, 700 and 710. Affected individuals from families 700 and 710 were homozygous for the R183W variant found in family 705. In family 312, we found another C-to-T transition (**Fig. 3c**), segregating in homozygosity with the disease, that would result in the replacement of threonine 54 with isoleucine (161C→T; T54I) in pejvakin. We did not detect the R183W and T54I variants in 200 chromosomes from normal-hearing Iranian controls.

Since DFNB27 and DFNB59 might be allelic disorders, we sequenced *DFNB59* in affected individuals belonging to the family that defined the *DFNB27* locus[11]. We did not detect any mutations in any of the *DFNB59* exons or splice sites in individuals with DFNB27 hearing impairment.

Pejvakin is a member of the DFNA5-gasdermin-MLZE protein family

We did not detect the existence of any signal peptides or transmembrane segments using computer-assisted analysis of the pejvakin sequence with different algorithms. Screening for sequence patterns predicted the existence of a nuclear localization signal (residues 249–258) and, with low scoring, a possible zinc-binding, DNA-interacting motif (residues 305–331) (**Fig. 4**).

We found *DFNB59* orthologs solely in vertebrate genomes (chimpanzee, rhesus monkey, mouse, rat, dog, cow, opossum, chicken, *Xenopus laevis*, zebrafish, *Fugu rubripes* and *Tetraodon nigroviridis*). Multiple sequence alignments showed that the two altered residues, T54 and R183, in DFNB59 subjects are conserved among all pejvakin orthologs.

Notably, BLAST database searches showed that pejvakin bears a significant similarity to DFNA5, a protein of unknown function altered in autosomal dominant nonsyndromic hearing impairment[12]. Alignments of pejvakin and DFNA5 sequences showed that similarity is confined to the respective N-terminal regions, with 32% identical and 54% similar residues over a stretch of 250 amino acids (data not shown). Exon organization in the two genes throughout the similarity region is identical (data not shown), indicating that pevjakin and DFNA5 share a common origin.

DFNA5 belongs to a family of proteins[13], found only in vertebrates, that also includes the gasdermins (GSDM1, GSDC1 and GSDML), involved in alopecia in mouse[14,15], and MLZE (melanoma-expressed, leucine zipper–containing extranuclear factor). Multiple sequence alignments indicated that pejvakin was a new member of this family and that it was the one most closely related to DFNA5 (**Supplementary Fig. 2** online). We analyzed sequence conservation and solvent accessibility in the family using the CONSEQ web server[16]. This analysis predicted that Thr54 in human pejvakin is exposed to solvent and, because of its conservation throughout the family, suggested that Thr54 has a functional role (**Fig. 4**). Arg183 was also predicted to be exposed to solvent; notably, although Arg183 is less well conserved throughout the family, none of the 53 homologs of pejvakin known to date harbors a tryptophan in the position equivalent to that of Arg183 in human pejvakin (**Supplementary Fig. 2** online).

Auditory neuropathy in *Dfnb59* R183W knock-in mice

To further substantiate the role of *DFNB59* mutations in DFNB59 auditory neuropathy, we generated two independent knock-in mouse lines harboring the same R183W variant in exon 3 of *Dfnb59* (approved allele designation is *Dfnb59*^{tm1Ugds}) by homologous recombination techniques. *Dfnb59*$^{tm1Ugds/tm1Ugds}$ mice from both lines were born at the expected mendelian frequency and showed

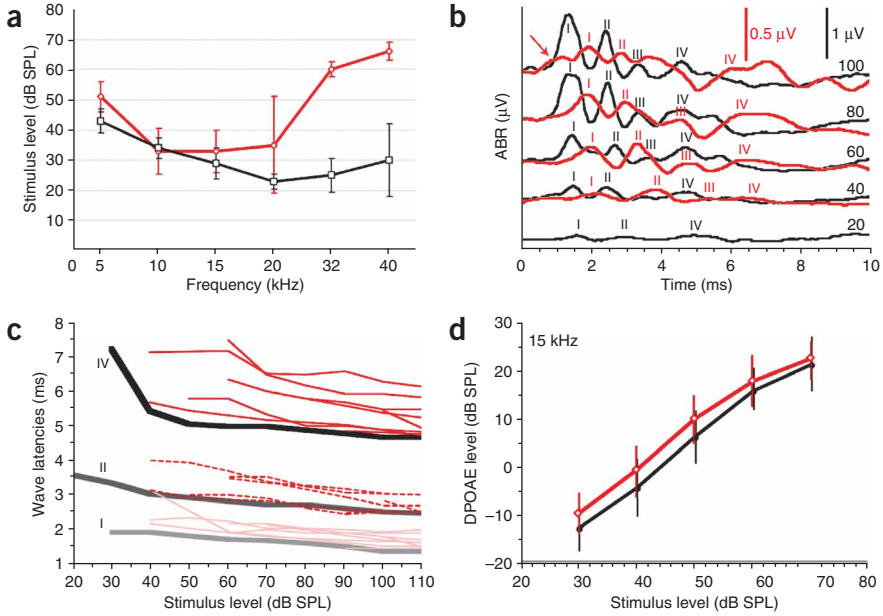

Figure 5 Audiological characterization of postnatal day 30 *Dfnb59* knock-in mice. (**a**) Mean ABR thresholds of eight wild-type (black) and eight *Dfnb59*$^{tm1Ugds/tm1Ugds}$ (red) mice of mixed C57BL/6-129/Sv background versus sound frequency. (**b**) Example of ABR waveforms at 20 kHz in one ear of a wild-type mouse (black) superimposed on an example of ABR waveforms in one ear of a *Dfnb59*$^{tm1Ugds/tm1Ugds}$ mouse (red). Waves I–IV are marked. Waveforms elicited at different hearing levels are offset for clarity. Labels at right indicate stimulus levels (in dB SPL). Arrow indicates wave peak corresponding to electrical activity of hair cells as shown by the delay in wave I at stimulus levels over 90 dB. (**c**) Wave latency as a function of stimulus intensity at 20 kHz for the three more robust ABR waves (I, II and IV). Black and gray lines mark upper limit of normative range in wild-type control mice of the same genetic background for waves I, II and IV. Red lines show results in individual ears from *Dfnb59*$^{tm1Ugds/tm1Ugds}$ mice with an ABR threshold elevation of >15 dB (pink lines, wave I; dashed lines, wave II; solid red, wave IV). At all frequencies tested, wave latencies in knock-in mice are longer than maximum latency observed in wild-type control littermates. (**d**) DPOAE growth functions at 15 kHz of ears from wild-type ($n = 8$; black) and *Dfnb59*$^{tm1Ugds/tm1Ugds}$ mice with an ABR threshold elevation of >15 dB at 15 kHz ($n = 6$; red). Differences in the DPOAE growth functions between wild-type and *Dfnb59*$^{tm1Ugds/tm1Ugds}$ mice are not significant. Vertical bars: ± 1 s.e.m.

no differences in growth, development or fertility from their *Dfnb59*$^{+/+}$ or *Dfnb59*$^{+/tm1Ugds}$ littermates. We did not observe any balance defects in *Dfnb59*$^{tm1Ugds/tm1Ugds}$ mice, indicating that their vestibular functions are normal. In addition, tests for motor coordination and for perception of touch and pain did not uncover any anomalies in *Dfnb59*$^{+/tm1Ugds}$ or *Dfnb59*$^{tm1Ugds/tm1Ugds}$ mice.

We analyzed the auditory functions of 18 *Dfnb59*$^{tm1Ugds/tm1Ugds}$ mice, on both pure 129/Sv (ten mice) and mixed C57BL/6-129/Sv (eight mice) genetic backgrounds, by recording ABRs and distortion-product OAEs (DPOAEs). When compared with their *Dfnb59*$^{+/+}$ and *Dfnb59*$^{+/tm1Ugds}$ littermates, all postnatal day (P) 30 *Dfnb59*$^{tm1Ugds/tm1Ugds}$ mice consistently showee an increase in their ABR thresholds at high frequencies (32–40 kHz); we observed the highest increase (35–45 dB) in mice from mixed C57BL/6-129/Sv genetic background (**Fig. 5a**). In all mice tested, threshold elevation correlated with abnormal shapes and reduced amplitudes of all ABR waves at the affected frequency (**Fig. 5b**). In particular, the absolute latencies of all four ABR waves and the interpeak latencies for waves I-II (auditory nerve) and III-IV (brainstem) were significantly augmented (**Fig. 5b,c** and **Table 1**), indicating conduction anomalies in the corresponding afferent auditory neurons. In a fraction of mutant mice, the increase in ABR thresholds extended into the middle-frequency range (2 of 18) or encompassed all frequencies (2 of 18). We recorded normal DPOAEs from mutant mice at the affected frequencies (**Fig. 5d**). Altogether, these results led us to conclude that the hearing impairment observed in *Dfnb59* knock-in mice qualifies as auditory neuropathy.

We next tested whether the hearing impairment in *Dfnb59* knock-in mice is progressive. As the 129/Sv inbred strain of mice exhibits age-related hearing loss (owing to cochlear hair cell death), which is evident in the high frequencies (>16 kHz) as early as 3 months of age[17], we performed this study in mice from the mixed C57BL/6-129/Sv background. The audiological parameters of C57BL/6-129/Sv *Dfnb59*$^{tm1Ugds/tm1Ugds}$ mice remained stable up to 8 months of age, which implies that this form of auditory neuropathy is non-progressive.

In view of the similarity between pejvakin and Dfna5 protein sequences, we explored whether inactivation of *Dfna5* would modify the phenotype of *Dfnb59* knock-in mice. We obtained *Dfna5*$^{-/-}$ *Dfnb59*$^{tm1Ugds/tm1Ugds}$ double mutants by crossing C57BL/6-129/Sv *Dfnb59*$^{tm1Ugds/tm1Ugds}$ mice with CBA/Ca *Dfna5*$^{-/-}$ mice[18]. The auditory phenotypes of *Dfnb59*$^{tm1Ugds/tm1Ugds}$*Dfna5*$^{+/+}$ and *Dfna5*$^{-/-}$ animals were indistinguishable, indicating that lack of Dfna5 did not have any effect on the hearing impairment of *Dfnb59*$^{tm1Ugds/tm1Ugds}$ mice (see **Supplementary Note**).

We performed exhaustive morphological analyses of the cochleae of *Dfnb59*$^{tm1Ugds/tm1Ugds}$ mice at different ages by means of light microscopy examination of cochlear semithin sections (data not shown) and scanning electron microscopy (**Supplementary Fig. 3** online). We also examined the morphology of the brainstem in *Dfnb59* knock-in mice (data not shown). We did not observe any structural abnormalities.

Table 1 Absolute and interpeak latencies of ABR waves in *Dfnb59*$^{tm1Ugds/tm1Ugds}$ mice and wild-type control littermates of the same genetic background

ABR wave	Latencies in wild-type littermates (ms)	Latencies in *Dfnb59*$^{tm1Ugds/tm1Ugds}$ mice (ms)	*P* (Mann-Whitney test)
I	<1.40	1.50–1.95	< 0.05
II	<2.50	2.50–3.55	< 0.05
III	<3.40	3.40–4.55	< 0.05
IV	<4.60	4.80–6.10	< 0.05
I-II	1.10	1.00–1.60	< 0.05
II-III	0.90	0.90–1.00	Not significant
III-IV	1.20	1.40–1.55	< 0.05

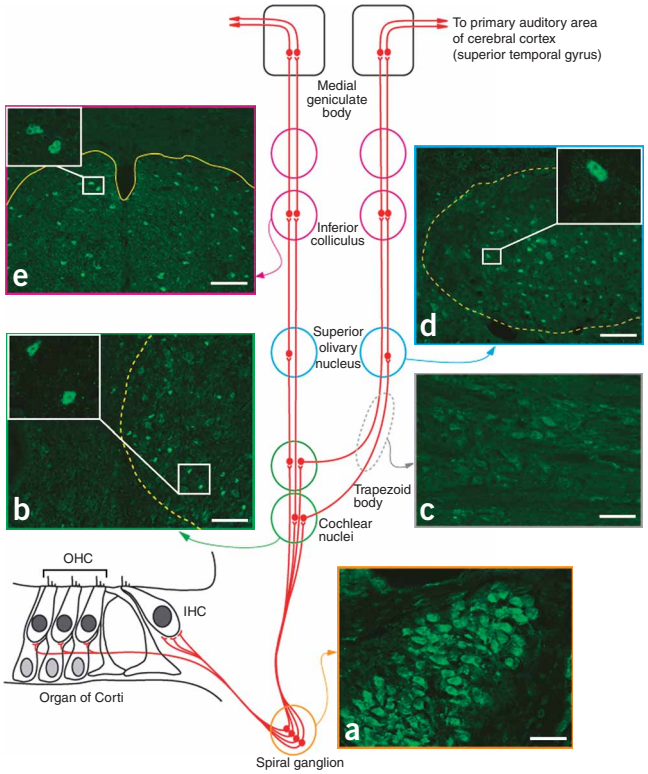

Figure 6 Expression of pejvakin in the afferent auditory system of P30 mice from pure 129/Sv genetic background. The block diagram shows the main ascending pathways that project both ipsilaterally and contralaterally (for the sake of clarity, only projections from one cochlea are presented). Images show expression of pejvakin in the soma of neurons located in the spiral ganglion (**a**), cochlear nuclei (**b**), superior olivary complex (**d**) and inferior colliculus (**e**). Pejvakin expression was not detected in fiber bundles, such as the trapezoid body (**c**). Although pejvakin expression is detected all spiral ganglion neurons, only a subset of neurons in brainstem auditory nuclei show pejvakin labeling, as indicated by coimmunolabeling with neuronal marker NeuN on adjacent sections (data not shown). Scale bars: 10 μm (**a**,**c**) and 50 μm (**b**,**d**,**e**).

Expression of pejvakin in the inner ear and auditory pathway

RT-PCR analysis detected *Dfnb59* transcripts in all the adult mouse organs tested: brain, eye, inner ear, heart, lung, kidney, liver, intestine, testis and weakly in skeletal muscle (data not shown).

We raised polyclonal antibodies (in rabbit and guinea pig) directed against peptides of mouse pejvakin in order to monitor its expression in the auditory system by immunofluorescence. We detected pejvakin expression in the organ of Corti (**Supplementary Note** and **Supplementary Fig. 4** online) and the spiral ganglion within the cochlea in the sensory areas of the vestibule (cristae ampullares of the semicircular ducts, and maculae of the saccule and utricle) and in the first three relays (cochlear nuclei, superior olivary complex and inferior colliculus) of the afferent auditory pathway.

In the afferent auditory pathway, we always observed pejvakin staining in the cell bodies of neurons (**Fig. 6**), with no labeling evident in fiber bundles such as the trapezoid body in the brainstem (**Fig. 6c**). We detected pejvakin in spiral ganglion cells (**Fig. 6a**), which form the auditory nerve and project to the cochlear nuclei in the brainstem. Pejvakin labeling was also observed in each of the following relays**:** the cochlear nuclei (**Fig. 6b**), the superior olive (**Fig. 6d**) and the inferior colliculus (**Fig. 6e**). We did not observe any differences in these pejvakin labeling patterns between wild-type and *Dfnb59*$^{tm1Ugds/tm1Ugds}$ mice.

DISCUSSION

We have shown in this work that missense mutations in a newly discovered gene, *DFNB59*, cause nonsyndromic, prelingual, severe-to-profound sensorineural hearing impairment, which fits the diagnostic criteria for auditory neuropathy. The *DFNB59* gene lies within the critical interval for *DFNB27* (**Fig. 1d**), a locus for prelingual, severe-to-profound deafness with autosomal recessive inheritance for which published clinical data are sparse[11]. We did not detect any mutations in *DFNB59* exons or splice junctions in DFNB27 affected individuals, which suggests that the causative genes in the two forms of hearing impairment are distinct. However, we cannot formally exclude the possibility that DFNB27 affected individuals harbor mutations in upstream regulatory sequences of the *DFNB59* gene that were not screened. Additional clinical characterization, such as recording ABRs and OAEs, of DFNB27 affected individuals may help resolve whether DFNB27 and DFNB59 are allelic disorders.

We have corroborated the role of *DFNB59* in hearing impairment by generating knock-in mice whose high-frequency auditory neuropathy mimics that observed in humans. Discrepancies between the phenotype of *Dfnb59* knock-in mice (ABRs with delayed but discernible waves) and the clinical manifestations observed in DFNB59 affected individuals (ABRs absent or with only a delayed wave V present) probably reflect subtle differences between the two species in the molecular physiology of the auditory pathway. Histological examination of the cochlea, the auditory nerve and the brainstem of *Dfnb59*$^{tm1Ugds/tm1Ugds}$ mice does not indicate any gross morphological abnormalities or pathological processes such as demyelination, implying that the hearing defect in those mice is functional, and not structural, in its origin. Comparison of the audiological data of *Dfnb59* knock-in mice and DFNB59 subjects uncovers two common features of interest.

First, cochlear hair cell function is preserved. The persistence of normal OAEs in both human subjects and *Dfnb59* knock-in mice shows that OHCs are functional. In addition, several lines of evidence indicate that IHC function is also spared. The stapedial reflex (a contraction of middle-ear muscles, prompted by acoustic overstimulation, that reduces sound transmission to the cochlea) is preserved in some humans with DFNB59. Because the stapedial reflex depends on acoustic information collected by IHCs and relayed by spiral ganglion neurons[3], we must conclude that IHCs are functional in those individuals. Moreover, the delay in ABR wave I in *Dfnb59*$^{tm1Ugds/tm1Ugds}$ mice at levels above 90 dB sound pressure level (SPL) shows a wave corresponding to the early electrical responses of hair cells (**Fig. 5b** and **Supplementary Fig. 5** online), which are usually masked by ABR wave I. As a substantial part of that early response stems from the electrical activity of IHCs[19], the presence of the unmasked wave with a normal size indicates that IHC receptor potentials are normal. Indeed, the persistence of functional IHCs in the mouse must be related to the fact that pejvakin was never detected in adult IHCs.

Second, DFNB59 human subjects and *Dfnb59* knock-in mice show impaired neural transmission of auditory information. Increases in wave V latency in humans are paralleled by comparable increases in both the absolute and interpeak ABR wave latencies in *Dfnb59* knock-in mice. Notably, some DFNB59 affected individuals with absent ABRs have measurable audiometric hearing levels. An explanation for this phenomenon stems from the fact that the ABR records the averaged response of many neurons in each relay

along the afferent auditory pathway[6]. A successful ABR recording requires that the timing of the neural discharges be almost identical after each of the test stimuli, whereas dys-synchrony in neural firing is believed to disrupt the averaged response so that it becomes unrecognizable[20]. Further proof for dys-synchrony comes from those subjects with recordable hearing levels in which an ABR wave V is present without discernible waves I or III. Likewise, wave IV is wider in *Dfnb59*$^{tm1Ugds/tm1Ugds}$ mice, implying that synchronous firing of neurons is impaired. In the auditory system, timing of the action potentials of neurons conveys the information essential to interpret and localize sound[21]; therefore, dys-synchrony severely undermines the ability of the cortical auditory centers to decode the sound signal.

Taken together, these characteristics strongly suggest that the primary lesion in DFNB59 hearing impairment is not located in the cochlea. Rather, our data support a dysfunction taking place in neurons along the auditory pathway, which is consistent with the observed distribution of pejvakin in the cell bodies of neurons in the spiral ganglion and the brainstem auditory nuclei. Thus, we conclude that pejvakin is essential in the activity of auditory pathway neurons. On the basis of its subcellular localization, attractive hypotheses include roles for pejvakin in the propagation of the action potential or in intracellular trafficking.

Of note, it is uncertain whether the missense mutations identified in this work abolish pejvakin function. Therefore, it is conceivable that other *DFNB59* mutations may result in different clinical entities, including syndromic deafness. Generation of *Dfnb59* knockout mice should help clarify this issue and provide further data on pejvakin function.

The term auditory neuropathy, because of its current operational definition, encompasses various conditions with widely different etiologies. These include neonatal insults (anoxia and hyperbilirubinemia), infectious processes (mumps and meningitis) and genetic factors[10,20], which together account for 7–10% of all childhood permanent hearing impairment[5,20]. Such etiologic diversity hinders proper clinical management of affected individuals. Indeed, cochlear implants (prosthetic electrode arrays inserted in the cochlea to directly stimulate the auditory nerve) are currently considered the most successful treatment for auditory neuropathy[20]. However, the outcome of cochlear implantation in each auditory neuropathy subject is uncertain owing to the diverse causes involved[9,20]. Thus, a more comprehensive evaluation of individuals with auditory neuropathy has been urged in order to accurately identify the anatomical location of their lesions[22]. So far, only one other gene, *OTOF*, encoding otoferlin[23], has been shown to be involved in nonsyndromic auditory neuropathy[24,25]. Although retrospective analysis has shown that cochlear implantation in individuals with an impairment due to *OTOF* mutations is completely successful[25], the underlying defect remains to be elucidated through the generation of an appropriate mouse model. Progress in identifying genes involved in nonsyndromic auditory neuropathy thus provides clinicians with a new, powerful diagnostic tool to distinguish among its heterogeneous causes. Then, the insights into the pathogenic processes derived from the analysis of animal models for these newly identified monogenic conditions, such as the model reported in this work, should help clinicians decide on the suitability of performing implantation in each particular case.

METHODS

Family data. Clinical examination was performed on a total of 12 affected subjects: three male subjects and one female subject (age 12–19 years) from family 705 and three male and five female subjects (age 16–23 years) from family 312. Pure-tone audiometry was carried out to evaluate air and bone conduction. Binaural mean pure-tone average of thresholds for air conduction (in dB SPL) was calculated for audiometric frequencies 0.5, 1 and 2 kHz ($PTA_{0.5,\ 1,\ 2\ kHz}$). Hearing impairment was additionally assessed by means of ABRs and SSOAEs. Otoscopic examination and tympanometry with acoustic reflex testing were performed systematically to rule out any conductive hearing impairment.

Genotyping and linkage analysis. This study was conducted with the approval of the INSERM Ethics Committee. Informed consent was obtained from all the subjects included in the study or from their parents. DNA was extracted from peripheral blood samples by standard procedures. Subjects were genotyped for a set of 400 microsatellite markers evenly spaced at 10- to 12-cM intervals throughout the genome (ABI Prism Linkage Mapping Set 2, Applied Biosystems). Lod scores were calculated by using the MLINK program of the FASTLINK computer package[26]. We assumed that hearing impairment was inherited in a fully penetrant, autosomal recessive mode, with a disease allele frequency of 0.001. Allele frequencies of polymorphic markers and meiotic recombination frequencies of males and females were assumed to be equal.

Mutation screening of *DFNB59* affected individuals. We identified candidate genes in the region of shared homozygosity, delimited by markers D2S138 and D2S324, by querying the NCBI and UCSC human genome databases. PCR primers were designed to amplify across all intron-exon boundaries of candidate genes, including *DFNB59* (**Supplementary Table 1** online). Amplified PCR products were sequenced in an ABI 3100 sequencer (Applied Biosystems).

Cloning of a full-length *DFNB59* cDNA. Mouse *Dfnb59* cDNA was obtained by 5′ RACE PCR performed on an oligo(dT)-primed, double-stranded cDNA library prepared with vestibular mRNA, extracted from postnatal day 1 (P1) 129/Sv mice[27]. Human *DFNB59* cDNA was reconstructed by RACE-PCR performed on a human testis cDNA library, with primers designed according to the sequence of human GenBank EST BQ887979. Mouse and human PCR products were cloned into the pCR2.1-TOPO vector (Invitrogen) and sequenced.

Sequence analyses. A search for sequence patterns (including zinc binding motifs) was performed with the SMART web server[28]. The nuclear localization signal was predicted by the PREDICTNLS algorithm[29]. The search for pejvakin homologs was initiated by a BLASTP search against the SWISSPROT database. This search clarified that pejvakin was paralogous to members of the protein family that includes DFNA5, the gasdermins and MLZE[13]. The orthologs of these different proteins were collected from the ENSEMBL database, release 36, as well as from all fully sequenced eukaryote genomes by using BLAT[30]. All retrieved proteins sequences were multiply aligned using MUSCLE[31], and the alignment was manually refined. The resulting alignment was used as input in the CONSEQ web server[16] to study the conservation pattern of pejvakin. In addition, the multiple sequence alignment was used in the creation of a phylogenetic tree using the PHYML algorithm[32].

Construction of *Dfnb59*$^{tm1Ugds/tm1Ugds}$ knock-in mice. We subcloned a 9.4-kb fragment of 129/Sv mouse genomic DNA, which included *Dfnb59* exons 1 to 4, using gap-repair homologous recombination[33] on BAC 310E9 from the CITB-CJ7B mouse BAC library (Research Genetics). To prepare the targeting vector, we introduced the R183W variant at the end of exon 3, a floxed *PGK-neo* G418-resistance cassette and a negative selection cassette coding for diphtheria toxin A fragment (*DTA*) (**Supplementary Fig. 6** online), by means of bacterial recombinogenic engineering techniques[34]. CK 35 embryonic stem (ES) cells[35], derived from a 129/Sv embryo, were electroporated with the purified, linearized targeting vector and plated on G418 selective medium as reported[36]. Two independently obtained ES cell clones, in which one *Dfnb59* wild-type allele had been replaced with the *Dfnb59*^{tm1Ugds} allele, were used to generate chimeric mice by injection into C57BL/6 host blastocysts. The floxed *PGK-neo* cassette was then removed by crossing *Dfnb59*$^{+/tm1Ugds}$ mice with *PGK-Cre* deleter mice[37].

Characterization of *Dfnb59*$^{tm1Ugds/tm1Ugds}$ mice. Animal experiments were carried out in accordance with the INSERM animal welfare guidelines, approved by the French Ministère de l'Agriculture, de l'Alimentation, de la Pêche et de la Ruralité. All studies described were performed on both pure 129/Sv and mixed C57BL/6-129/Sv genetic backgrounds. Balance tests were conducted as described[38]. Auditory tests, which consisted of DPOAEs, ABRs and cochlear potentials, were performed in an anechoic room. Mice were deeply anaesthetized by an intraperitoneal injection of ketamine chlorhydrate (3.5 mg for a 15-g mouse, renewed as needed), initially administered with levomepromazin chlorhydrate (0.1 mg). Cubic DPOAEs were elicited by a Cub^{e}Dis system (Mimosa Acoustics, v2.43) whose acoustic probe tip and calibration were modified to fit a mouse ear. Frequency f2 was swept at one-tenth-octave steps from 4 to 20 kHz (levels increased stepwise from 30–70 dB SPL). Input-output curves, representing DPOAE levels at every tested f2 against stimulus intensity, were plotted; averaged across wild-type, heterozygous and homozygous mutant mice; and compared using one-way ANOVA. ABRs were collected in response to calibrated short tone bursts in the 5–40 kHz range. The electroencephalogram was recorded between subcutaneous stainless steel electrodes at the vertex and ipsilateral mastoid, with the help of a standard digital averaging system. At every sound level, synchronous averaging of 500 responses to the tone bursts was performed. Well above threshold, ABRs consisted of at least four regularly spaced waves (I to IV, at increasing post-stimulus onset latencies), and wave IV was the last to disappear at near-threshold levels. ABR morphology was assessed while tone burst levels varied stepwise from 10–110 dB SPL peak-equivalent in 5-dB steps, and ABR threshold was taken to be the smallest stimulus level needed for producing at least one repeatable wave IV >0.3 μV.

Antibodies and immunocytofluorescence. We raised polyclonal antibodies (Covalab) directed against synthetic peptides mixtures of mouse pejvakin in rabbit and guinea pig. Peptide sequences were as follows: pejvakin-1 (19–33), NH_2-RLVPVPSLSEADKYQ-COOH; pejvakin-2 (312–323), NH_2-GMGNLKRETVYG-COOH. The specificity of the affinity-purified antibodies was verified by immunoblotting, immunostaining in HeLa cells that expressed pejvakin-myc epitope fusion proteins, and antigen absorption assays. All pejvakin antibodies gave similar staining patterns in immunofluorescence experiments both in transfected HeLa cells producing pejvakin and in mouse cochlear sections. Other primary antibodies used were as follows: mouse monoclonal antibodies to myc epitope (9E10; Santa Cruz), and to acetylated tubulin (C-11B-1; Sigma), rat monoclonal antibody to tyrosinated tubulin (YL1/2; Chemicon). For immunofluorescence detection, we used the following secondary antibodies: Alexa Fluor 488–conjugated goat anti-rabbit F(ab′)$_2$ IgG fragment (Molecular Probes), Cy3-conjugated sheep anti-mouse IgG (Amersham), Alexa Fluor 488–conjugated goat anti-guinea pig IgG (Molecular probes) and Cy3- conjugated donkey anti-rat F(ab′)$_2$ IgG fragment (Jackson ImmunoResearch). HeLa cells were transiently transfected with Effectene (Qiagen) and processed for immunocytofluorescence as reported[39].

Inner ear morphology studies. For both light and electron microscopy studies, inner ears from adult mice were fixed by perilymphatic perfusion with 2.5% phosphate-buffered glutaraldehyde. Specimens were subsequently rinsed in PBS buffer, decalcified in 0.35 M EDTA and immersed in 1% OsO_4 at 4 °C for 1 h. For light microscopy studies, inner ears from three *Dfnb59*$^{tm1Ugds/tm1Ugds}$ mice were then dehydrated through graded acetone solutions and embedded in Durcupan resin. Tissue sections (1 μm thick) were stained with toluidine blue and examined in a Leica optical microscope. Inner ears from a total of 11 *Dfnb59*$^{+/+}$ mice (nine at P30, one at P50, one at P75), five *Dfnb59*$^{+/tm1Ugds}$ mice (one at P15, two at P50, two at P75) and 21 *Dfnb59*$^{tm1Ugds/tm1Ugds}$ mice (three at P15, 13 at P30, three at P50, two at P75) were analyzed by scanning electron microscopy. Tissue specimens (including the cristae of semicircular ducts and the maculae of the saccule and utricle) from glutaraldehyde-fixed inner ears were microdissected, dehydrated in graded ethanol solutions and dried up to a critical point. Processed specimens were then mounted on aluminum stubs with colloidal silver adhesive and sputter-coated with gold palladium before imaging in a JSM-6700 F Jeol scanning electron microscope.

Inner ear immunofluorescence analyses. For whole-mount preparations, vestibular and cochlear sensory areas were dissected and processed as described[39]. We carried out isolated hair cell staining as previously reported[40]. Whole-mount and single cell preparations were analyzed on a Zeiss LSM540 laser scanning confocal microscope.

Brain immunohistofluorescence analyses. Adult mice (P30) were injected with a lethal dose of ketamine chlorhydrate and perfused intravascularly with PBS buffer, followed by 4% phosphate-buffered paraformaldehyde. The brain was excised and fixed in 4% phosphate-buffered paraformaldehyde for 1 h at 4 °C. After fixation, the tissue was cryoprotected in 20% sucrose at 4 °C overnight. The brain was then frozen in dry ice-cooled isopentane at –30 ° to –50 °C. We cut 14 μm-thick sections in the transversal plane in a Leica CM3000 cryostat and processed them for immunofluorescence as described[39].

URLs. The NCBI, UCSC and ENSEMBL genome databases are available at http://www.ncbi.nlm.nih.gov, http://genome.ucsc.edu/, and http://www.ensembl.org, respectively. The CONSEQ web server can be found at http://conseq.bioinfo.tau.ac.il/. The PHYML web server is at http://atgc.lirmm.fr/phyml/.

Accession codes. GenBank: human *DFNB59* cDNA, DQ365827; mouse *Dfnb59* cDNA, DQ365828.

Note: Supplementary information is available on the Nature Genetics website.

ACKNOWLEDGMENTS

The authors are grateful to all the families and clinicians involved in the study for their collaboration. We thank the staff at the Pasteur Institute of Iran and the Specialized Education Centers for their help in collecting subject samples; T. Hutchin and R.F. Mueller for generously sharing DNA samples from individuals belonging to the family that defined the *DFNB27* locus; N.G. Copeland for gifts of bacterial strains and plasmids; S. Nouaille, S. Chardenoux and F. Thouron for technical help; P. Roux for advice on confocal microscopy; M. Cohen-Salmon and S. Safieddine for advice on immunohistofluorescence techniques; J. Levilliers and A. Hafidi for discussion and J.P. Hardelin for critical reading of the manuscript. S.D. is grateful for the support of the Letten Saugstad Foundation. F.J.d.C was a recipient of a Marie Curie postdoctoral fellowship. L.V.L. is a postdoctoral fellow of the Flemish Fonds voor Wetenschappelijk Onderzoek (FWO). This work was supported by the European Commission FP6 Integrated Project EuroHear (LSHG-CT-2004-512063) and by Fondation Louis-Jeantet.

COMPETING INTERESTS STATEMENT

The authors declare that they have no competing financial interests.

Published online at http://www.nature.com/naturegenetics
Reprints and permissions information is available online at http://npg.nature.com/reprintsandpermissions/

1. Liberman, M.C. Single-neuron labeling in the cat auditory nerve. *Science* **216**, 1239–1241 (1982).
2. Rubel, E.W. & Fritzsch, B. Auditory system development: primary auditory neurons and their targets. *Annu. Rev. Neurosci.* **25**, 51–101 (2002).
3. Rouiller, E.M. Functional organization of the auditory pathways. in *The Central Auditory System* (eds. Ehret, G. & Romand, R.) 3–96 (Oxford Univ. Press, Oxford, 1997).
4. Romand, R. Modification of tonotopic representation in the auditory system during development. *Prog. Neurobiol.* **51**, 1–17 (1997).
5. Sininger, Y.S. Identification of auditory neuropathy in infants and children. *Semin. Hear.* **23**, 193–200 (2002).
6. Dirks, D.D., Morgan, D.E. & Ruth, R.A. Auditory brainstem response and electrocochleographic testing. in *The Ear: Comprehensive Otology* (eds. Canalis, R.F. & Lambert, P.R.) 231–241 (Lippincott Williams & Wilkins, Philadelphia, 2000).
7. Kemp, D.T. Otoacoustic emissions, their origin in cochlear function, and use. *Br. Med. Bull.* **63**, 223–241 (2002).
8. Starr, A., Picton, T.W., Sininger, Y.S., Hood, L.J. & Berlin, C.I. Auditory neuropathy. *Brain* **119**, 741–753 (1996).
9. Cone-Wesson, B. & Rance, G. Auditory neuropathy: a brief review. *Curr. Opin. Otolaryngol. Head Neck Surg.* **8**, 421–425 (2000).
10. Starr, A., Sininger, Y.S. & Pratt, H. The varieties of auditory neuropathy. *J. Basic Clin. Physiol. Pharmacol.* **11**, 215–230 (2000).
11. Pulleyn, L.J. *et al.* A new locus for autosomal recessive non-syndromal sensorineural hearing impairment (*DFNB27*) on chromosome 2q23-q31. *Eur. J. Hum. Genet.* **8**, 991–993 (2000).
12. Van Laer, L. *et al.* Nonsyndromic hearing impairment is associated with a mutation in *DFNA5*. *Nat. Genet.* **20**, 194–197 (1998).
13. Katoh, M. & Katoh, M. Identification and characterization of human DFNA5L, mouse Dfna5l, and rat Dfna5l genes in silico. *Int. J. Oncol.* **25**, 765–770 (2004).

14. Runkel, F. *et al.* The dominant alopecia phenotypes Bareskin, Rex-denuded, and Reduced Coat 2 are caused by mutations in *gasdermin 3*. *Genomics* **84**, 824–835 (2004).
15. Lunny, D.P. *et al.* Mutations in gasdermin 3 cause aberrant differentiation of the hair follicle and sebaceous gland. *J. Invest. Dermatol.* **124**, 615–621 (2005).
16. Berezin, C. *et al.* CONSEQ: the identification of functionally and structurally important residues in protein sequences. *Bioinformatics* **20**, 1322–1324 (2004).
17. Zheng, Q.Y., Johnson, K.R. & Erway, L.C. Assessment of hearing in 80 inbred strains of mice by ABR threshold analyses. *Hear. Res.* **130**, 94–107 (1999).
18. Van Laer, L. *et al.* Mice lacking Dfna5 show a diverging number of cochlear fourth row outer hair cells. *Neurobiol. Dis.* **19**, 386–399 (2005).
19. Durrant, J.D., Wang, J., Ding, D.L. & Salvi, R.J. Are inner or outer hair cells the source of summating potentials recorded from the round window? *J. Acoust. Soc. Am.* **104**, 370–377 (1998).
20. Rance, G. Auditory neuropathy / dys-synchrony and its perceptual consequences. *Trends Amplif.* **9**, 1–43 (2005).
21. Oertel, D. The role of timing in the brain stem auditory nuclei of vertebrates. *Annu. Rev. Physiol.* **61**, 497–519 (1999).
22. Rapin, I. & Gravel, J. "Auditory neuropathy": physiologic and pathologic evidence calls for more diagnostic specificity. *Int. J. Pediatr. Otorhinolaryngol.* **67**, 707–728 (2003).
23. Yasunaga, S. *et al.* A mutation in *OTOF*, encoding otoferlin, a FER-1-like protein, causes DFNB9, a nonsyndromic form of deafness. *Nat. Genet.* **21**, 363–369 (1999).
24. Varga, R. *et al.* Non-syndromic recessive auditory neuropathy is the result of mutations in the otoferlin (*OTOF*) gene. *J. Med. Genet.* **40**, 45–50 (2003).
25. Rodríguez-Ballesteros, M. *et al.* Auditory neuropathy in patients carrying mutations in the otoferlin gene (*OTOF*). *Hum. Mutat.* **22**, 451–456 (2003).
26. Schaffer, A.A. Faster linkage analysis computations for pedigrees with loops or unused alleles. *Hum. Hered.* **46**, 226–235 (1996).
27. Cohen-Salmon, M., El-Amraoui, A., Leibovici, M. & Petit, C. Otogelin: a glycoprotein specific to the acellular membranes of the inner ear. *Proc. Natl. Acad. Sci. USA* **94**, 14450–14455 (1997).
28. Letunic, I. *et al.* SMART 4.0: towards genomic data integration. *Nucleic Acids Res.* **32**, D142–D144 (2004).
29. Cokol, M. *et al.* Finding nuclear localization signals. *EMBO Rep.* **1**, 411–415 (2000).
30. Kent, W.J. BLAT–the BLAST-like alignment tool. *Genome Res.* **12**, 656–664 (2002).
31. Edgar, R.C. MUSCLE: a multiple sequence alignment method with reduced time and space complexity. *BMC Bioinformatics* **5**, 113 (2004).
32. Guindon, S. & Gascuel, O. A simple, fast and accurate algorithm to estimate large phylogenies by maximum likelihood. *Syst. Biol.* **52**, 696–704 (2003).
33. Lee, E.C. *et al.* A highly efficient *Escherichia coli*-based chromosome engineering system adapted for recombinogenic targeting and subcloning of BAC DNA. *Genomics* **73**, 56–62 (2001).
34. Liu, P., Jenkins, N.A. & Copeland, N.G. A highly efficient recombineering-based method for generating conditional knockout mutations. *Genome Res.* **13**, 476–484 (2003).
35. Kress, C., Vandormael-Pournin, S., Baldacci, P., Cohen-Tannoudji, M. & Babinet, C. Nonpermissiviness for mouse embryonic stem (ES) cell derivation circumvented by a single backcross to 129/Sv strain: establishment of ES cell lines bearing the Omd conditional lethal mutation. *Mamm. Genome* **9**, 998–1001 (1998).
36. Matise, M.P., Auerbach, W. & Joyner, A. Production of targeted embryonic stem cell clones. in *Gene Targeting: a Practical Approach* (ed. A. Joyner) 101–132 (Oxford Univ. Press, Oxford, 1999).
37. Lallemand, Y., Luria, V., Haffner-Krausz, R. & Lonai, P. Maternally expressed *PGK-cre* transgene as a tool for early and uniform activation of the Cre site-specific recombinase. *Transgenic Res.* **7**, 105–112 (1998).
38. Steel, K.P. & Hardisty, R. Assessing hearing, vision and balance in mice. in *What's Wrong With My Mouse? New Interplays Between Mouse Genes and Behavior* 26–38 (Society for Neuroscience, Washington D.C., 1996).
39. Küssel-Andermann, P. *et al.* Vezatin, a novel transmembrane protein, bridges myosin VIIA to the cadherin-catenins complex. *EMBO J.* **19**, 6020–6029 (2000).
40. Adato, A. *et al.* Interactions in the network of Usher syndrome type 1 proteins. *Hum. Mol. Genet.* **14**, 347–356 (2005).